Epitaxial strain and magnetic anisotropy in ultrathin Co films on W(110)

H. Fritzsche, J. Kohlhepp, and U. Gradmann
Physikalisches Institut, Technische Universität Clausthal, D 38678 Clausthal-Zellerfeld, Germany
(Received 17 November 1994)

The role of epitaxial strain for the anisotropies of ultrathin films is studied experimentally for the case of Co(0001) films on W(110), based on the measurement of anisotropies using torsion oscillation magnetometry combined with measurement of the strain by high-angular-resolution low-energy electron diffraction. Up to a thickness of $t=2$ nm, the films grow in a state of constant strain, governed by pseudomorphism in the direction ($[1\bar{1}00]$Co$\|[1\bar{1}0]$W), which results in a true volume-type strain anisotropy. Above 2 nm, a relaxation of strain is observed which scales roughly with $1/t$ and therefore results in an apparently surface-type contribution to strain anisotropy, superimposed on a reduced volume contribution. In-plane and out-of-plane volume and surface-strain anisotropies are calculated from the observed strain. For the four anisotropy constants, their calculated differences between the two regimes above and below 2 nm agree with their differences as determined by magnetometry.

I. INTRODUCTION

Magnetism in ultrathin films is characterized by strong and specific anisotropies. The evaluation of their origin is one of the major current issues in magnetic materials. At least three types of anisotropies are superimposed on the usual magnetocrystalline anisotropy: The ubiquitous shape anisotropy which forces the film magnetization into the film plane, Néel-type magnetic surface (interface) anisotropy (MSA) resulting from the broken symmetry in the surface (interface),[1] and strain anisotropy resulting from the epitaxial strain, which in turn is induced in the epitaxial film by interaction with a misfitting substrate. Most attention has been given during the last years to MSA, in particular for the case of "perpendicular" MSA,[2–4] which supports perpendicular magnetization and may, in ultrathin films, even overcome shape anisotropy and then result in perpendicular magnetization. However, perpendicular magnetization can be induced by strain anisotropies as well.[5–7] The present paper is concerned with the question in how far strain anisotropies in ultrathin films can be separated from the experimental data and in how far they can be explained, using concepts of bulk magnetoelasticity, from the strain which is determined by independent measurement.

For the separation of different anisotropy contributions, one starts from the fact that MSA is proportional to the film area A, virtually independent of magnetic film thickness t. It is therefore common use to separate MSA by plotting the total film anisotropy versus t, or the anisotropy density versus $1/t$, and then to obtain MSA from the axial section or from the slope, respectively. However, other anisotropies also contain contributions which scale with $1/t$ and therefore appear phenomenologically as surface contributions. Two types of such apparent surface anisotropies can be simulated by volume-type anisotropies which scale with $1/t$. (i) The decrease of magnetization with decreasing t, at finite temperatures, being proportional to $1/t$,[8] results in a *magnetostatic shape contribution* to MSA (Refs. 9 and 10) which is roughly proportional to temperature T. It is discussed in detail in Sec. V A below. (ii) The elastic strain in epitaxial films frequently relaxes with increasing thickness t following $1/t$, at least in some range of thickness and to some approximation. Chappert and Bruno[11] noted that this results in a *magnetoelastic strain relaxation contribution* to MSA. This strain relaxation contribution, which is an apparent MSA too, must be clearly distinguished from the true *magnetoelastic strain contribution* to MSA which has been discussed recently by O'Handley and coworkers.[12–14] It results if magnetoelastic coupling coefficients at surfaces are substantially different from their bulk values. The understanding of this O'Handley-type magnetoelastic strain contribution, which can be considered as a strain-induced contribution to the true Néel-type MSA, is in a pioneering state. In the case of our films, the available data do not allow its separation from the zero strain Néel-type MSA. We therefore dispense with its separate treatment and consider it as part of the Néel-type MSA. Some minor discrepancies in the final results may be connected with this contribution, as will be discussed in Sec. VI.

Strain anisotropies in ultrathin films may show up phenomenologically either as volume anisotropies for thickness regimes of constant strain, or as apparent surface-type strain relaxation anisotropies in regimes of relaxing strain. For their separation from true Néel-type MSA, it therefore turned out to be useful to study medium misfit epitaxial systems like Ni on Cu ($f_{\mathrm{NiCu}}=-2.5\%$) or Co on Cu ($f_{\mathrm{CoCu}}=-1.8\%$), for which the growing films are pseudomorphic (coherent) with the substrate up to some critical thickness t_c,[5,15–17] somewhere between 1 and 2 nm for Ni and Co on Cu (depending on the crystallographic orientation). For $t<t_c$, the films are in a state of constant strain, independent on t. Strain anisotropies then are pure volume type. Strain relaxation contributions to MSA are absent, the Néel -type MSA is left and can be determined in this pseudomorphic range. For $t>t_c$, strain relaxation MSA is superimposed. A comparison of both ranges then allows one to determine both

contributions to MSA. This method of separating the bare Néel-type MSA was applied first to Co on Cu(111).[18] It has been applied recently in careful studies of Ni on Cu(111) (Ref. 6) and Cu(100),[6,7] resulting in a clear separation of Néel-type and magnetoelastic strain relaxation contributions to MSA. The experimental values of the latter agreed in sign and in order of magnitude with estimates derived from standard elasticity models of strain relaxation above t_c. An independent measurement of the relaxing strain however was not intended in these studies.

In the present work, we extend this method of separating different MSA contributions by comparing pseudomorphic with relaxing regimes of film thickness in two directions: First we combine the magnetometric measurement of the anisotropies with an independent measurement of the strain, by high-angular-resolution low-energy electron diffraction (HR-LEED), and subsequent calculation of strain anisotropies, to be compared with the measured values. Second, we extend the analysis to a system in which both out-of-plane and in-plane anisotropies are present, given by Co on W(110). It will be shown that in this system, like in Ni on Cu, a regime of constant strain is available which extends up to $t=2$ nm. This again enables the separation of strain relaxation MSA from true Néel-type and magnetostatic shape contributions. We finally end up with a comparative discussion of experimental results for in-plane and out-of-plane, volume and surface-type magnetic strain anisotropies in our film system with theoretical values, calculated independently from the measured strain.

Our present work is related to the pioneering work of Lee *et al.*[19] who analyzed magnetic anisotropies in Co/Au(111) and Co/Cu(111) superlattices based on measurement of the strain which was done by x-ray techniques. Different from our work, they could not use a thickness-regime of constant strain, which is not available in superlattices. In addition, in-plane anisotropies were absent in their homosymmetric epitaxial system.

Our paper is organized as follows: After a short description of the experimental conditions in Sec. II, we discuss in Sec. III growth and structure of the films and their quantitative evaluation using HR-LEED, ending up in a quantitative strain model. This strain model enables the calculation of strain anisotropies which is given in Sec. IV. The experimental determination of the anisotropies by torsion oscillation magnetometry [TOM (Ref. 9)] is presented in Sec. V, which includes a discussion of the magnetostatic shape contribution MSA and a comparison of calculated and measured strain anisotropies. The final discussion and our conclusions are given in Sec. VI.

II. EXPERIMENTAL

The experiments were performed in two separate UHV systems, both equipped with a torsion oscillation magnetometer [TOM (Ref. 9)] working *in situ* in UHV and in external fields up to 0.4 T, with multiple evaporation sources for preparation of epitaxial sandwiches composed of several metals, and with LEED and Auger electron spectroscopy for structural testing. The two UHV systems differ in the following facilities: In the first one [U-TOM I (Ref. 9)] magnetometry is possible during film growth, but at $T \geq 300$ K only, and the structure can be tested by LEED spot profile analysis using a HR-LEED system.[20] The second system [U-TOM II (Ref. 21)] is designed for TOM at lowered temepratures; magnetometry and film growth must be performed in separate stages of the system; standard LEED is available. Although all preparations and measurements of this study were done at room temperature (RT), we used both systems because at present they are equipped with W(110) crystals in different orientations. In U-TOM I, in which most experiments were performed, the external field is oriented along $[1\bar{1}0]$W, in U-TOM II along [001]W. Because the easy in-plane axis of the Co films is along ($[1\bar{1}00]$Co$\|[1\bar{1}0]$W), we used samples in U-TOM I for the measurement of magnetic moment and of out-of-plane anisotropies from easy axis loops. The samples in U-TOM II in turn were used to observe hard-axis loops and to obtain in-plane anisotropies from them.

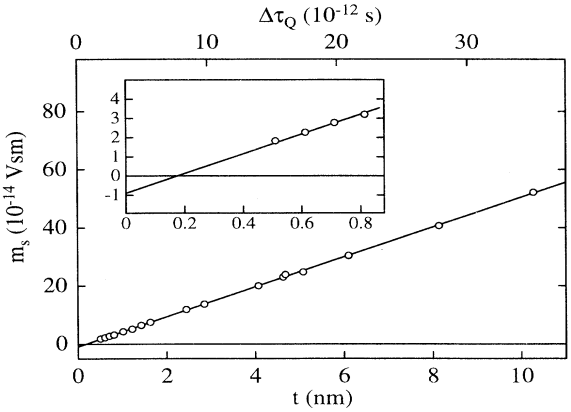

FIG. 1. Magnetic saturation moment m_s of Co(0001) films on W(110), plotted alternatively versus thickness t or versus the change $\Delta\tau_Q$ of the period of a simultaneously covered quartz-oscillator thickness monitor.

The thickness t of the Co films was determined in both systems with an accuracy below 0.1 ML by simultaneous evaporation of metals onto the sample and onto a water-cooled 10 MHz quartz oscillator crystal. This monitor was calibrated using TOM in the following way: The magnetic saturation moment m_s of the growing film was measured simultaneously with the change $\Delta\tau_Q$ of the period of the quartz oscillator, see Fig. 1. As expected, a linear dependence was observed. An increase of film thickness means an increase of the inner volume sections, with virtually constant (magnetic) properties of the surfaces. The linear increase therefore is connected with the bulk magnetization at RT, $J_s=1.82$ T.[22] Using the well-known film area A, we were able to determine $\Delta t=\Delta m_s/(J_s A)$ and therefore to unambiguously calibrate $\Delta\tau_Q$ versus t.

III. GROWTH, STRUCTURE, AND STRAIN STATE

Co films were prepared at RT with growth rates of the order of 0.1 nm/min on atomically smooth and clean

W(110) substrates, which were oriented with an accuracy better than 0.1° with respect to the surface normal. We followed the strain state of Co films on W(110) using HR-LEED up to a Co film thickness $t=6$ nm, alternatively speaking up to a number of (bulk) Co monolayers $D=t/0.20$ nm$=30$ ML. Up to roughly $D=4$ ML ($t=0.8$ nm), we confirmed structural findings which have been reported previously:[23–25] All films grew in the Nishiyama-Wassermann orientation, that means with the hexagonal base plane Co(0001) parallel to W(110), and $[11\bar{2}0]$Co$\|[001]$W. Figure 2 shows a superposition of undistorted bulk planes W(110) and Co(0001) in this orientation. For the description of the films, we use a Cartesian system with the x axis along ($[11\bar{2}0]$Co$\|$ [001]W), the y axis along ($[1\bar{1}00]$Co $\|[1\bar{1}0]$W), and the z axis along the film normal. Using the lattice parameters $a_W=0.3165$ nm and $a_{Co}=0.2507$ nm,[26] we obtain along the x axis a misfit $f_x=(a_{Co}-a_W)/a_W=-20.8\%$ and along the y axis a lower misfit $f_y=(\sqrt{3}a_{Co}-\sqrt{2}a_W)/\sqrt{2}a_W=-3.0\%$, both between bulk materials. Up to $D=0.7$ ML, the Co films show the (1×1) LEED pattern of the W(110) substrate. Accordingly, the Co film starts growing as a pseudomorphic monolayer. It is thermodynamically stable up to the desorption temperature of 1300 K.[23]

In the range between 1 and 4 ML Co, we observed the same LEED pattern as reported previously.[23–25] It is shown schematically in Fig. 3. Along the y axis, no splitting could be observed in this range. The films therefore are pseudomorphic in the y direction, with a homogeneous strain $\varepsilon_{22}=-(\sqrt{3}a_{Co}-\sqrt{2}a_W)/\sqrt{3}a_{Co}=+3.08\%$. In the x direction, we followed the strain state by measuring, using HR-LEED, the satellite splitting, given by b_2/b_1 as indicated in Fig. 3. From this, one easily calculates the strain $\varepsilon_{11}=[a_W b_1/a_{Co}b_2-1]$. Near the monolayer, we confirmed the previously[25] reported locking into a commensurate state with $b_1:b_2=4:5$, resulting in $\varepsilon_{11}=+1.00\%$. The monolayer is expanded in both in-plane directions. Above the monolayer, Knoppe and Bauer[25] reported a constant ratio $b_1:b_2=3.6:4.6$ for 2 ML $\leq D\leq 4$ ML, without giving an explanation for its magnitude. Using the enhanced sensitivity and accuracy of our HR-LEED, we could follow the satellites up to $D=8$ ML. Again, we found a constant (and slightly more accurate) value $b_1:b_2=3.56:4.56$, up to $D=8$ ML. Corresponding data of ε_{11} are included in Fig. 4. We obtain a mean value $\varepsilon_{11}=-1.45\%$ in this regime.

Beyond 8 ML, the satellites became invisible. ε_{11} therefore could not be followed from the satellite splitting. The strain below and above 8 ML could however be followed for the case of the y direction, by measuring the spot distance b_3, see Fig. 3. The strain ε_{22} can be easily calculated from b_3. The result is included in Fig. 4. As expected, ε_{22} is constant in the regime up to $t=1.8$ nm,

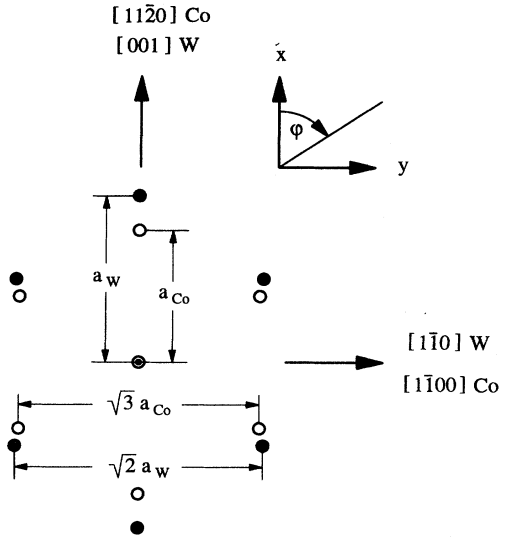

FIG. 2. Comparison of atomic positions in W(110) (solid circles ●) and Co(0001) (open circles ○). The figure shows positions in bulk lattice planes in Nishiyama-Wassermann orientation, $[11\bar{2}0]$Co$\|[001]$W. The misfits of Co with respect to W in the x and in the y direction are given by $f_x=(a_{Co}-a_W)/a_W=-20.8\%$ and $f_y=(\sqrt{3}a_{Co}-\sqrt{2}a_W)/\sqrt{2}a_W=-3.0\%$, respectively.

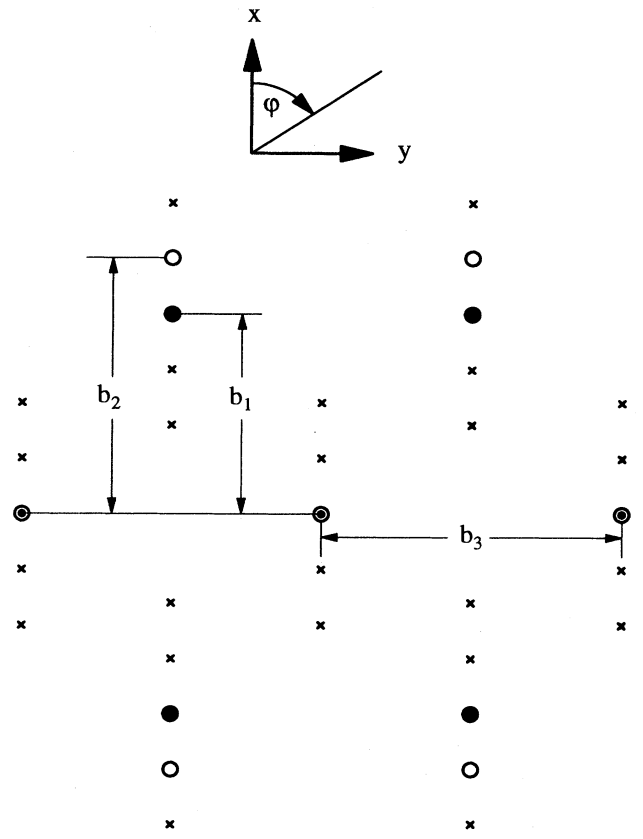

FIG. 3. Diffraction pattern of Co(0001) on W(110) in the regime between 1 and 4 monolayers Co, schematic. Spots of the W(110) substrate indicated by solid circles (●), spots of the distorted Co(0001) film by open circles (○), additional spots by crosses (×).

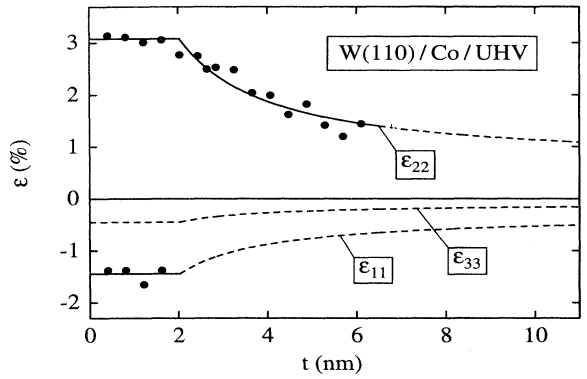

FIG. 4. Strain ε in an epitaxial Co(0001) film on W(110) versus thickness t. Experimental data for ε_{11} along $[11\bar{2}0]$Co and ε_{22} along $[1\bar{1}00]$Co are fitted by full lines using the strain model of Sec. III. Representation of the model completed by dotted lines.

and therefore can conveniently be normalized there to the pseudomorphic strain $\varepsilon_{22}=+3.08\%$. This has been done in Fig. 4. Above 2.0 nm, we observed a continuous outward shift of b_3, showing up in Fig. 4 as a relaxation of ε_{22} towards zero. This strain relaxation could be fitted by

$$\varepsilon_{22}=3.08\%[0.19+0.81(2.0\text{ nm}/t)] . \quad (1)$$

As seen in Fig. 4, the relaxing strain for large t crosses the constant strain $\varepsilon_{22}=3.08\%$ of the pseudomorphic regime at a critical film thickness $t_c=2$ nm, which is the upper limit of the pseudomorphic regime of constant strain.

It should be noted that all strain measurements strictly speaking are measurements of surface strain, because they are performed using HR-LEED. However, very general energetic rules tell us that the cores of misfit dislocation are situated in the very interface, that means in the first or probably in the second monolayer of the growing films.[27] It is therefore reasonable to identify the measured in-plane surface strain with the mean strain of the film, because the in-plane strain is expected to be homogeneous along the surface normal. This is assumed in what follows.

The strain information coming directly from our measurements can be completed in a straightforward manner as follows. Omitting from the present discussion the monolayer, we may distinguish two regimes, (I) a regime of constant strain for 0.4 nm $\leq t<2$ nm, and (II) a regime of strain relaxation for $t>2$ nm. In regime (I), the driving force for the constant strain is obviously the pseudomorphism along the y direction, resulting in $\varepsilon_{22}=+3.08\%$. It is then tempting to interpret the constant strain $\varepsilon_{11}=-1.45\%$ as a Poisson-type contraction resulting from the imposed expansion ε_{22}. We check this interpretation by calculating both Poisson contractions ε_{11} and ε_{33} using linear elasticity theory. By minimizing the elastic energy density[28]

$$f_{\text{el}}=(c_{11}/2)(\varepsilon_{11}^2+\varepsilon_{22}^2)+c_{12}\varepsilon_{11}\varepsilon_{22}$$
$$+(c_{33}/2)\varepsilon_{33}^2+c_{13}(\varepsilon_{11}+\varepsilon_{22})\varepsilon_{33} \quad (2)$$

for constant ε_{22} with respect to ε_{11} and ε_{33}, we obtain

$$\varepsilon_{11}=[(-c_{12}c_{33}+c_{13}^2)/(c_{11}c_{33}-c_{13}^2)]\varepsilon_{22} \quad (3)$$

and

$$\varepsilon_{33}=[(-c_{11}c_{13}+c_{12}c_{13})/(c_{11}c_{33}-c_{13}^2)]\varepsilon_{22} . \quad (4)$$

Using elastic constants $c_{11}=30.7\times10^{10}$ Nm^{-2}, $c_{12}=16.5\times10^{10}$ Nm^{-2}, $c_{13}=10.3\times10^{10}$ Nm^{-2}, and $c_{33}=35.8\times10^{10}$ Nm^{-2},[29] we obtain $\varepsilon_{33}=-0.45\%$ and $\varepsilon_{11}=-1.50\%$. The excellent agreement of the latter with the experimental value $\varepsilon_{11}=-1.45\%$ confirms its interpretation as a Poisson answer to ε_{22}, and therefore the applicability of continuum linear elasticity theory to our films. We conclude that the theoretical values of both ε_{11} and ε_{33} can be calculated from ε_{22} both below and above t_c.

As a result of the measurements and of the considerations given above we then obtain the following quantitative *strain model:*

(I) For 0.4 nm $<t<t_c=2.0$ nm we obtain $\varepsilon_{ii}^{(\text{I})}=\text{const}$ with $\varepsilon_{11}^{(\text{I})}=-1.50\%$, $\varepsilon_{22}^{(\text{I})}=+3.08\%$, $\varepsilon_{33}^{(\text{I})}=-0.45\%$.

(II) For $t>t_c=2.0$ nm, the strain components are given by

$$\varepsilon_{ii}^{(\text{II})}=\varepsilon_{ii}^{(\text{I})}[\alpha+(1-\alpha)(t_c/t)] , \quad (5)$$

with $\alpha=0.19$.

This model is visualized in Fig. 4. It will be used below for the calculation of strain anisotropies. It should be emphasized that Eq. (5) includes a constant residual strain contribution of $0.19\times\varepsilon_{ii}^{(\text{I})}$ which persists virtually for infinite t. The physical reason for this contribution is some energy barrier against the formation of a residual group of misfit dislocations which would be required to accommodate the residual infinite range epitaxial strain. Such a virtually constant epitaxial strain in thick films, superimposed on the leading $1/t$ contribution, has been reported previously for the cases of Ni on Cu(111) (Ref. 5) and of Ni on Cu(100).[15] We guess that it is a quite general consequence of the nonequilibrium properties of even the best epitaxial structures, which always are artificial, and that it could be detected in many other films by sufficiently careful measurements. Magnetically, it must show up in a volume-type contribution to strain anisotropy. This contribution is neglected in the Chappert-Bruno model[11,30] of strain-relaxation-induced MSA because the model is based on equilibrium considerations. Strain-relaxation-induced MSA therefore is overestimated in this model, at the expense of a long-range volume-type strain anisotropy, which is neglected in the equilibrium model, but is typical for real films because they are artificial nonequilibrium structures.

IV. STRAIN ANISOTROPY

The calculation of magnetoelastic coupling energy for a given strain, that means of magnetic strain anisotropy,

is a straightforward but tedious task, even in the usual second-order approximation, in which it has been solved for the present case of Co(0001) by Bruno.[31,28] Higher-order approximations are not available, to our knowledge. The unavoidable omission of fourth-order terms is a severe restriction because fourth-order terms are needed both for the description of crystalline volume anisotropies and of Néel-type surface anisotropies.[32–34] For the magnetoelastic energy density we write in this second-order approximation

$$f^{\rm me}=K^{\rm me}\cos^2\vartheta+K_p^{\rm me}\sin^2\vartheta\cos^2\varphi\ , \tag{6}$$

where ϑ and φ are the polar angle of magnetization direction with respect to the surface normal (z axis), and its azimuth with respect to the x axis $[11\bar{2}0]$Co, respectively. We assume that the strain tensor is diagonal in the Cartesian system of Fig. 2. With the usual magnetoelastic constants B_i, we then obtain from Bruno's work an out-of-plane magnetoelastic anisotropy constant

$$K^{\rm me}=-B_1\varepsilon_{22}-B_2\varepsilon_{33}-B_3(\varepsilon_{11}+\varepsilon_{22}) \tag{7}$$

and an in-plane anisotropy constant

$$K_p^{\rm me}=B_1(\varepsilon_{11}-\varepsilon_{22})\ . \tag{8}$$

Using Eq. (5), we write

$$K^{\rm me}=K_v^{\rm me}+(1/t)K_s^{\rm me} \tag{9a}$$

and

$$K_p^{\rm me}=K_{v,p}^{\rm me}+(1/t)K_{s,p}^{\rm me} \tag{9b}$$

as superpositions of appropriate volume and surface contributions. Taking the elastic constants[29] and magnetostriction constants[35] of bulk Co, one obtains $B_1=-0.81\times10^7$ J/m^3, $B_2=-2.90\times10^7$ J/m^3, $B_3=2.82\times10^7$ J/m^3.[28] Using these values, and the strain values from the model of the last section, we obtain the magnetoelastic anisotropy constants $K_v^{\rm me}$ and $K_s^{\rm me}$ which are shown in Table I for both regimes I and II. Surface contributions of course disappear in the initial regime I of constant strain. For comparison with the experiments to be described in the next section, we include the differences $\Delta K^{\rm me}=\Delta K^{\rm me}({\rm II})-\Delta K^{\rm me}({\rm I})$ between the constants in both regimes.

TABLE I. Out-of-plane anisotropy constants for Co films on W(110). Constants are given separately for thickness regimes (I) ($t<2$ nm) and II ($t>2$ nm). For the definition of the constants see Eqs. (7), (9a), (22), and (23). Magnetoelastic anisotropy constants $K_v^{\rm me}$ (line 1) of the volume and $K_s^{\rm me}$ (line 3) of the surfaces are calculated from the strain model of Sec. III. Experimental anisotropy constants ($K_v+K_{v,4yz}$) (line 2) and ($K_s+K_{s,4yz}$) (line 4) of volume and surface, respectively, are determined by TOM. The point of comparison is the difference ΔK for each constant between the values in regimes (I) and (II), respectively. Note the good agreement between the theoretical and the experimental differences, in particular for the volume constants.

			Regime I $t<2$ nm	Regime II $t>2$ nm	ΔK
1	$K_v^{\rm me}$	(10^5 J/m^3)	−3.3	−0.7	2.6
2	$K_v+K_{v,4yz}$		−7.6	−4.7	2.9
3	$K_s^{\rm me}$	(mJ/m^2)	0.0	−0.5	−0.5
4	$K_s+K_{s,4yz}$		0.1	−0.7	−0.8

V. MAGNETOMETRY AND EVALUATION OF ANISOTROPIES

Actual film anisotropies, to be compared with the data calculated from the observed strain, were measured *in situ* by torsion oscillation magnetometry (TOM).[5,36,33] In this method, we observe small amplitude torsion oscillations of the sample, near its equilibrium orientation with the magnetization parallel to the external magnetic field H. We measure a magnetic torque constant R as a function of H. This torque constant R is determined by the magnetic moment component m of the film along the field, by the saturation moment m_s, and by the second derivative $F_{\vartheta\vartheta}(\vartheta,\varphi)$ of the free energy with respect to the polar angle ϑ of the magnetization. Using an anisotropy field given by

$$H_{\rm anis}=F_{\vartheta\vartheta}/m_s\ , \tag{10}$$

one obtains[33]

$$R/H=m/(1+H/H_{\rm anis})\ . \tag{11}$$

This relation is exact for the case of an easy-axis loop, with $m=m_s$. For the case of a hard-axis loop, Eq. (11) gives $m=m(H)$ to a good approximation.

In the present Co(0001) films, the easy axis was oriented along ($[1\bar{1}00]$Co $\parallel$ $[1\bar{1}0]$W) (y axis of Fig. 2), which was the field axis in U-TOM I. Accordingly, magnetic saturation moment m_s and the out-of-plane anisotropy fields $H_{\rm anis}$ were determined in U-TOM I from easy-axis loops. The in-plane anisotropy was determined from hard-axis loops measured in U-TOM II.

We start our presentation in subsection (A) with the measurement and discussion of the magnetic moment. Quantitative evaluation will show that there is a strong decrease of m_s and therefore of shape anisotropy with decreasing t, showing up as a magnetostatic shape contribution to surface anisotropy. We discuss the determination of anisotropies in general in subsection (B).

A. Magnetic moment and the magnetostatic shape contribution to MSA

The magnetic saturation moment m_s of Co films on W(110), measured at room temperature, is shown in Fig. 1 versus t. As seen in particular from the inset, m_s follows a relation

$$m_s=J_s\,A(t-t_d)\ , \tag{12}$$

with an axial section $t_d=0.18$ nm, corresponding $D_d=0.9$ "dead layers." J_s is the bulk saturation magnetization. For $t\geq t_d$, the mean magnetization $J(t)=m_s/(At)$ therefore is given by

$$J(t)=J_s(1-t_d/t)\ . \tag{13}$$

A decrease of magnetization with decreasing thickness according to Eqs. (12) and (13) is typical for thin films.[17,9,8] The correction term $J_s \cdot t_d / t$ is the origin of an apparent surface-type contribution to shape anisotropy. The total magnetostatic energy (shape anisotropy) per area is given by

$$F_m / A = [(1/2\mu_0) \int J^2(z) dz] \cos^2\vartheta \ , \tag{14}$$

where $J(z)$ is the local magnetization. For the discussion of F_m, we first note that t_d can be caused either by a deviation of the ground-state magnetic moment per atom in the surface from its bulk value ("surface effect") or by the enhanced thermal decrease of magnetization in thin films ("size effect"). For the present case of Co, there is strong evidence of a far-reaching stability of the magnetic surface moment with respect to changes in the environment,[37] that means a small surface effect, which we neglect. For the resulting case of the bare size effect, it is well known that D_d is proportional to temperature T.[8] The present value $D_d = 0.9$ ML is of the same order of magnitude as has been observed previously[17] for the bare size effect in NiFe(111) on Cu(111) at the relative temperature of the present experiment, 0.22 T_c [$D_d = 0.6$ ML (Ref. 17)]. Of course, F_m depends on the details of the spatial structure $J(z)$. The situation is easy for ultrathin films with roughly $D \leq 4$ ML, for which the decrease of magnetization is homogeneous along the surface normal, as a result of strong exchange interactions.[8] This results in $\int J^2(z) dz = (J)^2 \cdot t$. Fortunately, the same relation applies for $D > 4$ ML and $T = 300$ K because the relative deviations of $J(z)$ from the mean value are small. As a result, the shape anisotropy per area for our films is given in general in a very good approximation by

$$F_m / A = [(J_s^2/2\mu_0)t - (J_s^2/\mu_0)t_d + (J_s^2 t_d^2/2\mu_0)/t] \cos^2\vartheta \ . \tag{15}$$

The first term in the brackets represents the usual shape anisotropy, which is proportional to t and is connected with the bulk saturation magnetization J_s. The third term can be mostly neglected. The second term is independent on t, as the true Néel-type MSA. In a phenomenological sense, it is therefore a magnetic shape contribution to MSA. As the magnetization change is composed by surface and size contributions, this magnetostatic shape contribution of MSA is composed of a true surface contribution, which is independent on T, and an apparent one, the size contribution, which is proportional to T. Independently of this distribution, the shape contribution to MSA is given by

$$K_s^{\rm sh} = -(J_s^2/\mu_0)t_d \ . \tag{16}$$

In our samples, it amounts to -0.47 mJ/m^2 for the film, or to -0.23 mJ/m^2 per interface. It may be overestimated a bit by completely attributing t_d to a size effect (in the limit of the pure surface effect, $K_s^{\rm sh}$ would be reduced by a factor of 2). Even then, $K_s^{\rm sh}$ would be of the standard order of MSA and therefore cannot be neglected in our case. For comparison, in the first paper in which the magnetostatic shape contribution to MSA was addressed, for the case of Ni films on Re,[10] it was a negligible correction of only 0.04 mJ/m^2 per interface, because of the low magnetization of Ni. In Fe films it is probably small, because the negative side contribution may be compensated to some degree by a positive surface contribution, resulting from the surface enhancement of magnetic moment.[38] For the present case of Co films, where the magnetization is both large and virtually unchanged in the surface, the magnetostatic shape contribution to MSA is of considerable magnitude. It has been mostly neglected so far in the literature and should be included in the future discussion.

B. Measurement and evaluation of anisotropies

As in our previous analysis of magnetic anisotropies of Fe(110) interfaces,[33] we use a fourth-order approximation both for the volume and for the surface contributions of $F(\vartheta,\varphi)$. Using directional cosines $\beta_1 = \sin\vartheta \cdot \cos\varphi$, $\beta_2 = \sin\vartheta \cdot \sin\varphi$, and $\beta_3 = \cos\vartheta$, we write for the free energy per volume

$$(1/V)F(\vartheta,\varphi) = [L\beta_3^2 + K_p\beta_1^2] + [K_{4xy}\beta_1^2\beta_2^2 + K_{4yz}\beta_2^2\beta_3^2 + K_{4xz}\beta_1^2\beta_3^2] \ , \tag{17}$$

where the second- and fourth-order anisotropy constants are composed of volume and surface contributions according to

$$L = [(J_s^2/2\mu_0) + K_v] + (1/t)K_s \ , \tag{18}$$

$$K_p = K_{v,p} + (1/t)K_{s,p} \ , \tag{19}$$

and

$$K_{4ik} = K_{v,4ik} + (1/t)K_{s,4ik} \ , \tag{20}$$

respectively.

For determining the out-of-plane anisotropy, we observe small amplitude oscillations with the magnetization along the easy axis $[1\bar{1}00]$Co (y axis), that means for $\vartheta = \varphi = \pi/2$, and therefore measure $F_{\vartheta\vartheta}(\pi/2,\pi/2)$. As has been shown in Ref. 33 [Eq. (13a)], the second derivative per area then is given by

$$(1/A)F_{\vartheta\vartheta}(\pi/2,\pi/2) = 2[L + K_{4yz}]t \ . \tag{21}$$

Using Eqs. (18) and (20), this becomes

$$(1/A)F_{\vartheta\vartheta}(\pi/2,\pi/2) = [(J_s^2/\mu_0) + 2(K_v + K_{v,4yz})]t + 2(K_s + K_{s,4yz}) \ . \tag{22}$$

In the present case, $K_v = K_v^{\rm cr} + K_v^{\rm me}$ is composed of a crystalline contribution $K_v^{\rm cr}$ and a magnetoelastic one, $K_v^{\rm me}$. Similarly, $K_s = K_s^{\rm Né} + K_s^{\rm sh} + K_s^{\rm me}$ is composed of Néel-type, shape, and magnetoelastic contributions $K_s^{\rm Né}$, $K_s^{\rm sh}$, and $K_s^{\rm me}$, respectively.

Accordingly, we finally obtain

$$(1/A)F_{\vartheta\vartheta}(\pi/2,\pi/2) = [(J_s^2/\mu_0)+2(K_v^{cr}+K_v^{me}+K_{v,4yz})]t + 2(K_s^{Né}+K_s^{sh}+K_s^{me}+K_{s,4yz}) . \quad (23)$$

Equations (22) and (23) are the basis for our evaluation of out-of-plane anisotropies. Note that a separation into different contributions is possible only for the second-order constants, whereas the fourth-order constants $K_{v,4yz}$ and $K_{s,4yz}$ contain all contributions, including the magnetoelastic one, which is out of the range of our quadratic approximation in Eq. (6). Experimental results for $(1/A)F_{\vartheta\vartheta}(\pi/2,\pi/2)$ versus t are shown in Fig. 5. As expected from the strain measurements, we observe two linear sections in regimes (I) ($t<2$ nm) and (II) ($t>2$nm), respectively. Volume and surface anisotropies can be taken for both regimes from slope and axial sections. Results for $K_v+K_{v,4yz}$ and $K_s+K_{s,4yz}$, obtained using Eq. (22), are included in Table I. The numerical values are obtained from a fit including the last term in the brackets of Eq. (15), which does not show up in the figure.

There is no reason why magnetocrystalline, shape, and Néel contributions to MSA should be different in both regimes, because it is only the strain state that makes their difference. Accordingly, the differences both of volume and surface anisotropies are expected to be differences in their strain contributions. The point of comparison between our experimentally determined anisotropies (lines 2 and 4 in Table I) and the strain anisotropies calculated from the measured strain (lines 1 and 3) is therefore given by their respective differences from both regimes. These differences ΔK between respective contributions of out-of-plane anisotropies from both regimes are included in the last column of Table I. We note a remarkably good agreement of ΔK_v^{me} as calculated from strain with the corresponding $\Delta(K_v+K_{v,4yz})$ from magnetometry, and fair agreement of the surface anisotropy changes ΔK_s^{me} with $\Delta(K_s+K_{s,4yz})$.

For the case of in-plane anisotropies, rough estimates only can be presented. They result from measurements in U-TOM II with the external field along the hard axis ([11$\bar{2}$0]Co ||[001]W) (x axis in Fig. 2). The problem of evaluating the in-plane anisotropies is explained by comparison of the hard-axis loops shown in Figs. 6(a) and 6(b). For the case of the 51 layers film in Fig. 6(a), the in-plane anisotropy field $H_p=2(K_p+K_{4xy})/J_s$ is small in comparison with the available external field. Accordingly, the crossing of the initial linear section of the loop $(R/H)/m_s$ with the saturation hyperbola $(R/H)/m_s = 1/(1+H/H_{anis})$ [see Eq. (11)] at H_p can be determined easily. For the case of the 7.9 layers film in Fig. 6(b), saturation could not be attained. A rough measure only of H_p can be obtained in this and similar cases by the section of the initial slope with $(R/H)/m_s=1$ [for the case of Fig. 6(b) we obtain $\mu_0 H_p=0.4$ T]. Experimental values of

$$(1/A)F_{\varphi\varphi}(\pi/2,\pi/2)=2(K_p+K_{4xy})t = 2(K_{v,p}+K_{v,4xy})t + 2(K_{s,p}+K_{s,4xy}) \quad (24)$$

versus t are shown in Fig. 7. Again, the two regimes below and above $t=2$ nm can be distinguished. Evaluation of the two straight lines results in the in-plane anisotropy constants for both regimes which are collected in Table II in connection with the calculated values of their magnetoelastic components. As for the out-of-plane anisotropies, the point of comparison between theory and

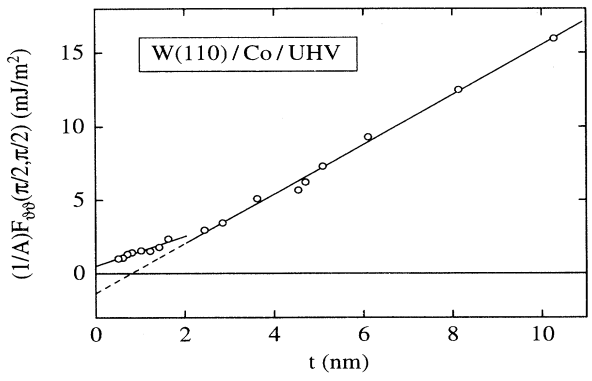

FIG. 5. Out-of-plane anisotropy $(1/A)F_{\vartheta\vartheta}(\pi/2,\pi/2)$ versus t for Co films on W(110).

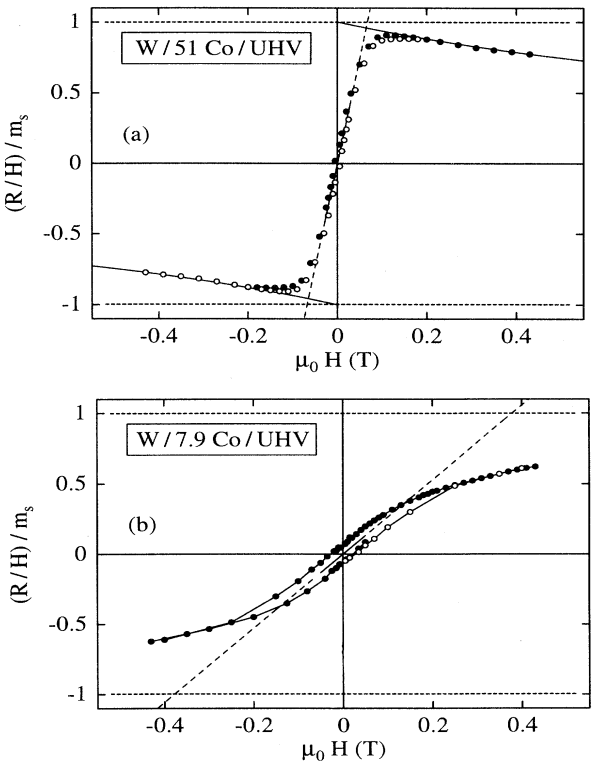

FIG. 6. Hard-axis magnetization loops $(R/H)/m_s$ versus H for two Co films on W(110), consisting of (a) 51 and (b) 7.9 monolayers, respectively. Solid circles represent true measurements, open circles are obtained by inversion from closed ones.

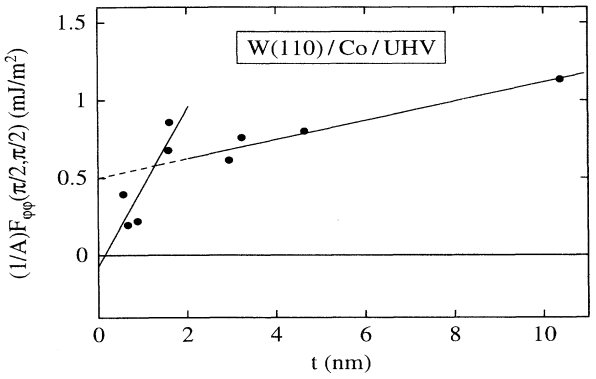

FIG. 7. In-plane anisotropy $(1/A)F_{\varphi\varphi}(\pi/2,\pi/2)$ versus t for Co films on W(110).

experiment must be the difference of anisotropy constants in both regimes. As shown by the last column, the agreement between calculated and measured values for those differences is again surprisingly good.

VI. DISCUSSION, SUMMARY, AND CONCLUSIONS

It was the main intention of the present paper to check in how far strain-induced magnetic anisotropies in ultrathin films can be separated from other anisotropy contributions and in how far they can be explained from the independently measured strain, using concepts of standard magnetoelastic continuum theory. As an experimental sample, we chose Co films on W(110), which offer the opportunity of analyzing both in-plane and out-of-plane anisotropies. The system provides a thickness-regime $t<2$ nm of constant strain (regime I), in which the strain anisotropies are constant too, that means they appear as true volume-type anisotropies, and therefore can easily be separated from the true Néel-type and shape contributions to MSA. For $t>2$ nm (regime II), the relaxing strain induces a relaxing strain anisotropy which is roughly proportional to $1/t$ and therefore shows up as an apparent MSA. Being physically a relaxing volume anisotropy, this contribution cannot be separated, in the relaxation regime II, from the Néel contribution $K_s^{\text{Né}}$, and is therefore treated as a relaxing strain contribution K_s^{me} to the phenomenologically defined MSA.

TABLE II. In-plane anisotropy constants for Co films in W(110). Constants are given separately for thickness regimes (I) ($t<2$ nm) and II ($t>2$ nm). For the definition of the constants see Eqs. (8), (9b), and (24). Magnetoelastic anisotropy constants $K_{v,p}^{\text{me}}$ (line 1) of the volume and $K_{s,p}^{\text{me}}$ (line 3) of the surfaces are calculated from the strain model of Sec. III. Experimental anisotropy constants $(K_{v,p}+K_{v,4xy})$ (line 2) and $(K_{s,p}+K_{s,4xy})$ (line 4) of volume and surface, respectively, are determined by TOM. The point of comparison is the difference ΔK for each constant between the values in regimes (I) and (II), respectively. Note the good agreement between the theoretical and the experimental differences, in particular for the volume constants.

			Regime I $t<2$ nm	Regime II $t>2$ nm	ΔK
1	$K_{v,p}^{\text{me}}$	(10^5 J/m^3)	3.7	0.8	−2.9
2	$K_{v,p}+K_{v,4xy}$		2.5	0.3	−2.2
3	$K_{s,p}^{\text{me}}$	(mJ/m^2)	0.0	0.6	0.6
4	$K_{s,p}+K_{s,4xy}$		0.0	0.3	0.3

The main results of our study are contained in Tables I and II. Before discussing them, we recall the limitations of our phenomenological ansatz of anisotropies: (i) For the description of strain anisotropies, only the second-order ansatz of Eq. (6) is available; higher-order terms are neglected. (ii) The dependence of the true Néel-type MSA on strain, as discussed by O'Handley, could not be included. (iii) Whereas the Co films can be assumed to be mainly hcp type,[25] some tendency to stacking faults must be considered. As discussed by Lee *et al.*,[19] magnetocrystalline anisotropies in hcp Co react sensitively on stacking faults, and the hcp values therefore must be taken with care, whereas the magnetoelastic constants react comparatively insensitively.

Having these limitations in mind, let us first discuss the out-of-plane anisotropies, given in Table I. Because Néel-type surface anisotropies of our films are unknown, and volume anisotropies are uncertain in view of limitation (iii), we cannot extract experimental values of the strain contributions from the experimental anisotropies given in Table I, lines 2 and 4, which could be compared with their values as calculated from measured strain, given in lines 1 and 3, respectively. The point of comparison therefore is given by the differences ΔK of anisotropy constants between regimes I and II, which we expect to result from the magnetoelastic contributions only. In comparing the experimental values of ΔK from lines 2 and 4 with the calculated ones in lines 1 and 3, we state a quite good agreement. The remaining minor differences can easily be explained from unknown corrections by higher-order contributions of f^{me} and from an unknown O'Handley-type dependence of K_s on strain. If we instead take the magnetoelastic constants from lines 1 as granted, we can determine $(K_v+K_{v,4yz}-K_v^{\text{me}})=-4.3\times10^5$ J/m^3 (from regime I) or -4.0×10^5 J/m^3 (from regime II). The agreement of both values is good. However, they deviate from what one would expect as a crystalline contribution in terms of usual anisotropy constants K_1 and K_2 of hcp Co, $(K_v^{\text{cr}}+K_{v,4yz}^{\text{cr}})=(-K_1-2K_2)=-7.2\times10^5$ J/m^3.[39] Apparently, $K_{v,4yz}=K_{v,4yz}^{\text{cr}}+K_{v,4yz}^{\text{me}}$ contains a magnetoelastic contribution $K_{v,4yz}^{\text{me}}$ in addition to the magnetocrystalline contribution $K_{v,4yz}^{\text{cr}}$. A modification of K_v by stacking faults must be considered too. In a similar way, we obtain from lines 3 and 4 values for $(K_s^{\text{Né}}+K_s^{\text{sh}}+K_{s,4yz})=(K_s+K_{s,4yz}-K_s^{\text{me}})$. Using $K_s^{\text{sh}}=-0.5$ mJ/m^2 from Sec. V A, we obtain $(K_s^{\text{Né}}+K_{s,4yz})=0.6$ mJ/m^2 (from regime I) or 0.3 mJ/m^2 (from regime II). The differences may be connected with limitations (i) and (ii).

The in-plane anisotropies given in Table II can be discussed in a similar way. Again, the point of comparison

is given by the respective differences of anisotropy constants between regimes I and II. Again, the agreement between the experimental differences in lines 2 and 4 and the calculated ones in lines 1 and 3, respectively, is quite good. In-plane magnetocrystalline volume anisotropies are absent in our samples because of the sixfold in-plane symmetry. The in-plane volume anisotropies therefore should be of pure magnetoelastic origin, which apparently is not the case, as seen from comparison of lines 1 and 2 in Table II. The differences between $K_{v,p}^{me}$ in line 1 and $(K_{v,p}+K_{v,4xy})$ in line 2 might be explained from higher-order contributions of f^{me}.

In conclusion, we analyzed the strain state in Co films on W(110) by HR-LEED. We established, for increasing thickness, a regime I of constant strain, followed by a regime II of relaxing strain. From this strain, magnetic strain anisotropies, both in-plane and out-of-plane, were calculated using standard magnetoelasticity theory. They show up in regime I as true volume anisotropies, in regime II as apparent surface anisotropies, superimposed by residual volume anisotropies. For comparison, we measured both in-plane and out-of-plane anisotropies using torsion oscillation magnetometry. Whereas it was not possible to extract the bare strain anisotropies from the measured film anisotropies, to be compared with the calculated ones, we took advantage of the fact that at the transition between regime I and II only the strain components of the film anisotropies are changed. Accordingly, we had to compare calculated and measured values of the changes of anisotropies between the two regimes. We found reasonable agreement of those differences for in-plane, out-of-plane volume and surface anisotropy contributions. For the minor differences, possible causes were discussed.

ACKNOWLEDGMENT

This work was supported by the Deutsche Forschungsgemeinschaft.

[1]L. Néel, J. Phys. Radium **15**, 225 (1954).
[2]U. Gradmann and J. Müller, Phys. Status Solidi **27**, 313 (1968).
[3]P. F. Carcia, A. D. Meinhaldt, and A. Suna, Appl. Phys. Lett. **47**, 178 (1985).
[4]F. J. A. den Broeder, W. Hoving, and P. J. H. Bloemen, J. Magn. Magn. Mater. **93**, 562 (1991).
[5]U. Gradmann, Ann. Phys. (Leipzig) **17**, 91 (1966).
[6]R. Jungblut, M. T. Johnson, J. a. de Stegge, A. Reinders, and F. J. A. den Broeder, J. Appl. Phys. **75**, 6424 (1994).
[7]B. Schulz and K. Baberschke, Phys. Rev. B **50**, 13 467 (1994).
[8]U. Gradmann, in *Handbook of Magnetic Materials,* edited by K. H. J. Buschow (Elsevier Science, Amsterdam, 1993), Vol. 7/1, p. 1.
[9]R. Bergholz and U. Gradmann, J. Magn. Magn. Mater. **45**, 389 (1984).
[10]U. Gradmann, R. Bergholz, and E. Bergter, IEEE Trans. Magn. **20**, 1840 (1984).
[11]C. Chappert and P. Bruno, J. Appl. Phys. **64**, 5736 (1988).
[12]S. W. Sun and R. C. O'Handley, Phys. Rev. Lett. **66**, 2798 (1991).
[13]G. Bochi, O. Song, and R. C. O'Handley, Phys. Rev. B **50**, 2043 (1994).
[14]O. Song, C. A. Ballentine, and R. C. O'Handley, Appl. Phys. Lett. **64**, 2593 (1994).
[15]J. W. Matthews and J. L. Crawford, Thin Solid Films **5**, 187 (1970).
[16]W. A. Jesser and J. W. Matthews, Philos. Mag. **17**, 46 (1968).
[17]U. Gradmann, Appl. Phys. **3**, 161 (1974).
[18]J. Kohlhepp, H. J. Elmers, and U. Gradmann, J. Magn. Magn. Mater. **121**, 487 (1993).
[19]C. H. Lee, H. He, F. J. Lamelas, W. Vavra, C. Uher, and R. Clarke, Phys. Rev. B **42**, 1066 (1990).
[20]U. Scheithauer, G. Meyer, and M. Henzler, Surf. Sci. **178**, 441 (1986).
[21]J. Kohlhepp, Ph.D. thesis, Technische Universitat Clausthal, 1994.
[22]R. Pauthenet, J. Appl. Phys. **53**, 8187 (1982).
[23]B. G. Johnson, P. J. Berlowitz, D. W. Goodman, and C. H. Bartholomew, Surf. Sci. **217**, 13 (1989).
[24]J. G. Ociepa, P. J. Schultz, K. Griffiths, and P. R. Norton, Surf. Sci. **225**, 281 (1990).
[25]H. Knoppe and E. Bauer, Phys. Rev. B **48**, 1794 (1993).
[26]R. W. G. Wyckoff, *Crystal Structures* (Wiley, New York, 1963), Vol. 1, p. 2.
[27]M. Przybylski and U. Gradmann, in *The Structure of Surfaces,* edited by J. F. v. der Veen and M. A. Van Hove (Springer, Berlin, 1988), Vol. II, p. 426.
[28]P. Bruno, in *Magnetismus von Festkörpern und Grenzflächen,* edited by P. H. Dederichs, P. Grünberg, and W. Zinn (Forschungszentrum Jülich, Jülich, 1993), Vol. 24, p. 24.1.
[29]H. J. McSkimin, J. Appl. Phys. **26**, 406 (1955).
[30]P. Bruno and J.-P. Renard, Appl. Phys. A **49**, 499 (1989).
[31]P. Bruno, J. Phys. F **18**, 1291 (1988).
[32]H. Fritzsche, J. Kohlhepp, H. J. Elmers, and U. Gradmann, Phys. Rev. B **49**, 15 665 (1994).
[33]H. Fritzsche, H. J. Elmers, and U. Gradmann, J. Magn. Magn. Mater. **135**, 343 (1994).
[34]H. Fritzsche, J. Kohlhepp, and U. Gradmann, J. Magn. Magn. Mater. (to be published).
[35]A. Hubert, W. Unger, and J. Kranz, Z. Phys. **224**, 148 (1969).
[36]U. Gradmann, W. Kümmerle, and R. Tham, Appl. Phys. **10**, 219 (1976).
[37]A. J. Freeman and R. Q. Wu, J. Magn. Magn. Mater. **104-107**, 1 (1992).
[38]U. Gradmann, G. Waller, R. Feder, and E. Tamura, J. Magn. Magn. Mater. **31-34**, 883 (1983).
[39]R. M. Bozorth, Phys. Rev. **96**, 311 (1954).